



Article

Finite Element Analysis-Aided Optimization of Rectangular Coil Assemblies Applied in Electric Vehicle Inductive Chargers

Guodong Zhu  and Dawei Gao *

State Key Laboratory of Automotive Safety and Energy, School of Vehicle and Mobility, Tsinghua University, Beijing 100084, China; jack.zg68@live.com

* Correspondence: dwgao@mail.tsinghua.edu.cn

Abstract: Energy efficiency and leakage magnetic field (LMF) are two important issues in electric vehicle inductive chargers. In this work, the maximum achievable coil efficiency and the corresponding LMF strength are formulated as functions of system parameters, and figures of merits (FOM) are proposed for assessing the efficiency and LMF performance of the coil assembly pair. The impacts of the coil assemblies' geometric parameters on both FOMs are examined with the aid of finite element analysis (FEA), and measures to improve the FOMs are suggested based on FEA results. A manual optimization process is conducted on a coil assembly pair. Compared with the initial design, the optimized one results in a higher DC-to-DC efficiency and lower LMF strength while consuming less copper. The performance improvement is verified by FEA results and experimental data measured on an 85 kHz electric vehicle inductive charger prototype. The key measures for coil assembly optimization are summarized.

Keywords: efficiency; electric vehicle; finite element analysis; inductive charger; optimization



Citation: Zhu, G.; Gao, D. Finite Element Analysis-Aided Optimization of Rectangular Coil Assemblies Applied in Electric Vehicle Inductive Chargers. *World Electr. Veh. J.* **2021**, *12*, 219. <https://doi.org/10.3390/wevj12040219>

Academic Editor: Hui Yang

Received: 12 September 2021

Accepted: 28 October 2021

Published: 4 November 2021

Publisher's Note: MDPI stays neutral with regard to jurisdictional claims in published maps and institutional affiliations.



Copyright: © 2021 by the authors. Licensee MDPI, Basel, Switzerland. This article is an open access article distributed under the terms and conditions of the Creative Commons Attribution (CC BY) license (<https://creativecommons.org/licenses/by/4.0/>).

1. Introduction

Efficiency improvement [1] and leakage magnetic field (LMF) suppression [2] are two important issues in inductive power transfer (IPT) systems, e.g., electric vehicle inductive chargers. The fundamental principle of IPT is to utilize the conversion between electrical energy and magnetic energy as a means of transmitting power over an air gap. Such a conversion is realized via a pair of coil assemblies, one on the transmitter (TX) side and the other on the receiver (RX) side; hence, the design of the coil assembly pair greatly influences the system performance. The simplest coil assembly pair consists of two single-winding circular coils having a spiral, rectangular or square shape. Multi-winding coils are proposed to enhance the performance from certain aspects, examples of which include the DD coil [3], the DDQ coil [4] and the solenoidal coil [5]. The increased complexity is an obvious shortcoming, though.

This work is focused on the coil assembly pair composed of two single-winding rectangular coils. The interoperability among different types of coils is of high practical value; however, it is not discussed here because its rich content simply cannot be fully covered in such a short article. The advantages of single-winding rectangular coils are that they are easy to manufacture and have the largest area under a given width-by-length dimensional constraint. Besides, it is a common practice to fabricate the ferrite core using multiple small ferrite bricks; hence, rectangular cores are easier to manufacture than circular ones. It is natural to pair a rectangular core with a rectangular coil.

The optimization of coil assemblies has been discussed in numerous references. Some previous works endeavored to maximize the coupling coefficient [6]. The dependency of the coupling coefficient on the geometric parameters is analyzed in [7] using the response surface methodology. Some tried to strike a balance among multiple objectives [8–10]. For most IPT systems, the latter, i.e., multi-objective optimization of the coil assemblies, is of more practical value as a practical IPT system is usually subject to various constraints.

Both analytical methods and numerical methods, e.g., finite element analysis (FEA) [6,8] and the finite-difference time-domain method (FDTD) [11,12], are useful tools for performance evaluation. Analytical methods are based on simplifications and are usually restricted to certain types of coil assembly designs [9]. They are practical tools for analyzing coil assemblies with simple geometric features, e.g., axis-symmetrical coils. When complex geometric features are included, the number of degrees of freedom to be considered in the model should be greatly increased to guarantee high accuracy, which actually obscures the main advantage of analytical methods, i.e., simplicity. By contrast, numerical methods are universally applicable and yield good results, provided that the model parameters are accurate and the software itself is based on solid physical foundations. Compared with simplified analytical methods, numerical methods generally consume more computing power. However, both the runtime and the hardware cost will be decreased with the evolution of technologies. A popular approach is to combine numerical methods with modern optimization methods, e.g., genetic algorithm, to obtain the optimal design in a systematic and efficient manner [6,8].

Two optimization methodologies that are commonly adopted in the literature are shown in Figure 1. Examples of analytical equation-based optimization are [5,9,13,14]. In [14], only the copper winding is considered, and the spiral coil is approximated using circular loops, which greatly reduces the number of degrees of freedom. In [9], the ferrite layer is modelled using a homogeneous layer, the number of decision variables is three and the impact of coil misalignment is omitted. In [13], the parameters of the lumped-loop analytical model, instead of the physical parameters of the coil assemblies, are utilized during parameter sweep, and the runtime is greatly reduced. In [5], a loss calculation method and a magnetic-circuit model for the solenoidal-type coil assemblies are proposed, and the turn numbers are optimized to maximize the energy efficiency. Examples of FEA-based optimization are [8,10]. In [10], the optimization is accomplished using a combination of FEA simulations and analytical equations. All possible combinations of design parameters are tested. In [8], FEA is combined with the particle swarm algorithm to test possible parameter combinations.

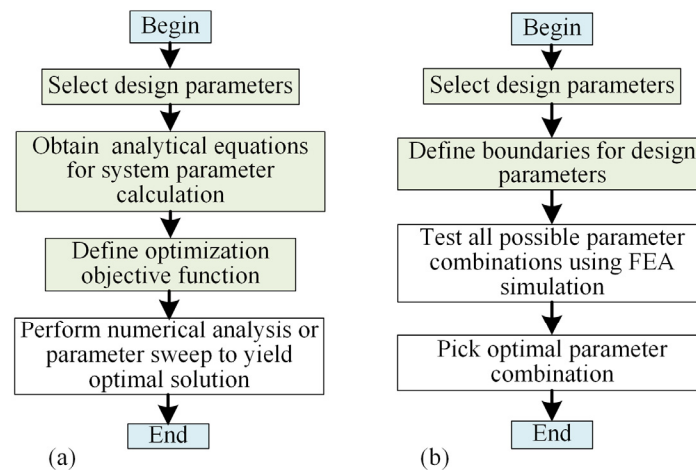


Figure 1. Optimization methodologies commonly adopted in the literature. (a) Analytical, equation-based optimization. (b) Finite element analysis-based optimization.

The dominant factors of energy efficiency are mutual inductance and coil ESRs (equivalent series resistance). In a typical electric vehicle inductive charger, a coil assembly contains three parts: an aluminum shielding plate, a ferrite core and copper winding. The eddy loss in the aluminum plate is related to the ambient magnetic flux density. According to the Steinmetz equation, which is commonly adopted for characterizing magnetic core loss under sinusoidal magnetic field excitations, core loss is approximately a power function of magnetic flux density. Copper loss is influenced by the DC resistance, skin effect,

proximity effect and other stray factors. When the strand diameter of Litz wire is below the skin depth, skin effect has a small impact. Proximity effect is related to the magnetic flux density that the copper winding is exposed to [13,15]. Under a given excitation current amplitude, all loss terms are affected by the geometric parameters of the coil assembly. Coil ESR is the combined effect of all three loss terms. Meanwhile, the output power is proportional to mutual inductance. Therefore, the maximum achievable energy conversion efficiency of the coil assembly pair (designated as η_c and abbreviated as “coil efficiency” in the remaining sections) is influenced by not only coil ESRs but also mutual inductance, and the difficulty in maximizing η_c lies in the fact that both are affected by the geometric parameters in complex ways. To objectively assess the efficiency performance of a coil assembly pair, figures of merits (FOMs) that reflect the combined influence of all relevant factors are a useful criterion [14]. Obviously, the η_c -FOM is determined by the geometric parameters of the coil assembly pair. Measures to improve η_c via coil assembly optimization have been extensively discussed in previous publications [8,10,14].

As for LMF suppression, the measures can be divided into two categories: active suppression [2] and passive shielding [16]. In active suppression schemes, extra coils are usually deployed to generate a magnetic field component that partially counteracts the field generated by the TX and RX coils, thus reducing the overall field strength to an acceptable level. Due to the extra hardware and software cost, such methods are more suitable for high-power applications where passive shielding alone is insufficient. By contrast, passive shielding techniques rely on the design of the coil assembly pair to reduce the leakage magnetic field strength and are widely adopted due to their simplicity and effectiveness. LMF suppression techniques generally have a negative impact on η_c , and efforts have been made to strike a balance between η_c and the LMF strength [8,10,13].

In this article, passive magnetic shielding alone is adopted. Two FOMs are proposed to assess the efficiency performance and the LMF performance of the coil assembly pair applied in electric vehicle inductive chargers. This work is focused on the ferrite layer structure and the copper winding parameters and aims to reveal the impacts of the geometric parameters on the FOMs via a combination of finite element analysis (FEA) and empirical knowledge. Qualitative rules regarding the impacts of geometric parameters are extracted, based on which a simple manual optimization procedure under given geometric constraints is conducted with the purpose of improving η_c while minimizing the impact on the LMF performance. The superiority of the optimized design is demonstrated through FEA results and experimental results obtained from an 85 kHz electric vehicle inductive charger prototype. The result is encouraging: the optimized design achieves significantly higher η_c and lower LMF strength while consuming less copper.

The remainder of this article is divided into the following sections. In Section 2, the maximum achievable η_c and the corresponding LMF strength are analyzed, and two FOMs are proposed for assessing the efficiency and LMF performance of a coil assembly pair. In Section 3, the overall design of the coil assemblies is introduced and the impacts of geometric parameters on the FOMs are derived from FEA results. The design parameters, i.e., the geometric parameters to be varied during the optimization process, are selected. In Section 4, the accuracy of FEA in terms of coil loss calculation is verified. Manual optimization of the coil assembly pair is conducted, and the superiority of the optimized design is validated by FEA results and experimental results. Section 5 gives some discussions. Section 6 concludes this article.

2. Performance Evaluation of Coil Assemblies

2.1. Efficiency Analysis

A simplified schematic of an IPT system with series compensation on both sides is shown in Figure 2. U_{in} is the inverter's output voltage, U_L is the voltage across the load resistance, I_1 and I_2 are the coil currents, C_1 and C_2 are the series compensation capacitors, L_1 and L_2 are the coil inductances, M is the mutual inductance, R_L is the equivalent AC load resistance and R_1 and R_2 are the coil ESRs. Considering that the focus of this work is

coil assembly optimization, the power losses in the other components are neglected. Due to the band-pass property of the compensation networks, only the fundamental voltages and currents are considered. For the sake of simplicity, coil ESRs are assumed to be zero except in efficiency calculations.

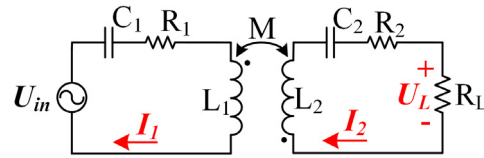


Figure 2. Simplified schematic of series-series-compensated IPT system.

Measures to maximize η_c have been discussed in numerous studies [1]. For the simplified IPT system shown in Figure 2, the output power (P_{out}) is

$$P_{out} = \frac{1}{2} I_1 \cdot (j\omega M I_2) \leq \frac{1}{2} \omega M |I_1| \cdot |I_2| \quad (1)$$

The power loss on coil ESRs is

$$P_{coil} = \frac{1}{2} (|I_1|^2 R_1 + |I_2|^2 R_2) \geq 2P_{out} \frac{\sqrt{R_1 R_2}}{\omega M} \quad (2)$$

The conditions for minimizing the P_{coil} -to- P_{out} ratio are

$$\angle I_1 - \angle I_2 = 90^\circ \quad (3)$$

$$|I_1|^2 R_1 = |I_2|^2 R_2 \quad (4)$$

The first condition is satisfied by maintaining the circuits in full resonance, i.e., $L_1 C_1 = L_2 C_2 = 1/\omega^2$, where ω is the angular operating frequency of the IPT system. In this work, the operating frequency is fixed at 85 kHz. Equation (2) reveals that the lowest achievable P_{coil} -to- P_{out} ratio is a function of $\frac{M^2}{R_1 R_2}$. In this article, this ratio is selected as the FOM for assessing the efficiency performance of the coil assembly pair and designated as FOM_{effi} . A larger FOM_{effi} means the maximum achievable η_c is higher. Meanwhile, the optimal AC load resistance that maximizes η_c is

$$R_{L,opt} = \frac{\omega M |I_1|}{|I_2|} = \omega M \sqrt{\frac{R_2}{R_1}} \quad (5)$$

2.2. Leakage Magnetic Field Analysis

LMF is defined as the magnetic field that users might be exposed to under predefined operating conditions, e.g., the magnetic field in the vicinity of an inductively charged electric vehicle. Under the assumption that the flux lines generated by both coil assemblies are overlapped in the LMF region [2], the LMF strength at a selected observation point under conditions (3) and (4) is simplified as

$$B_{LMF} = \sqrt{k_1^2 |I_1|^2 + k_2^2 |I_2|^2} = \sqrt{\frac{2P_{out}}{\omega M}} \sqrt{k_1^2 \sqrt{\frac{R_2}{R_1}} + k_2^2 \sqrt{\frac{R_1}{R_2}}} \quad (6)$$

where k_1 or k_2 denotes the magnetic flux density generated by 1 A coil current on the observation point. Therefore, the expression $M \cdot \left(k_1^2 \sqrt{\frac{R_2}{R_1}} + k_2^2 \sqrt{\frac{R_1}{R_2}}\right)^{-1}$ is selected as the FOM for assessing the LMF performance and designated as FOM_{LMF} . A larger FOM_{LMF} means the LMF strength at the maximum- η_c operating point is lower.

Generally speaking, B_{LMF} increases with coil misalignment, i.e., the highest B_{LMF} is observed when the vehicle-side coil is at the maximum-misalignment position. Still, the FOM_{LMF} calculated based on the k_1 and k_2 data measured at the zero-misalignment position is a useful indicator of the LMF performance. Overall, the LMF strength in the maximum-misalignment case has a positive correlation with that in the zero-misalignment case.

3. Influence of Geometric Parameters

3.1. Overall Design of Coil Assembly Pair

As is shown in Figure 3a, a ferrite layer is inserted between the copper winding and the aluminum shielding plate. FEA results reveal that under the same ferrite consumption limit, both core loss and eddy loss are minimized when an integral ferrite core, instead of separate ferrite strips with spaces between them, is adopted. In this work, protrusions are added along the outer contour of the ferrite layer to improve mutual inductance and reduce eddy loss. The top view of the coil assembly (excluding the aluminum plate) is given in Figure 3b.

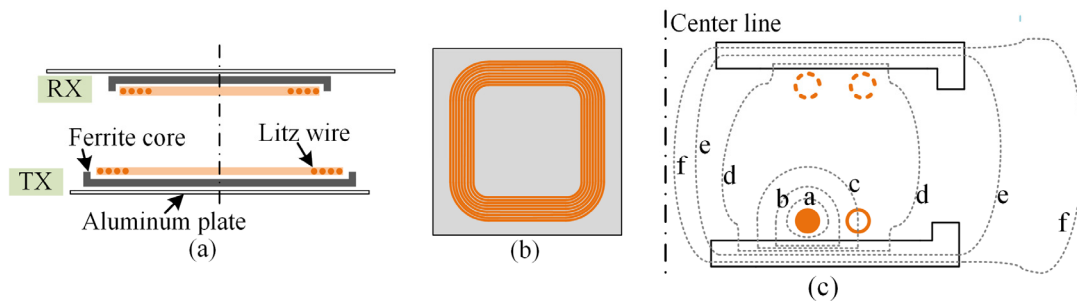


Figure 3. Overall design of the coil assemblies and the magnetic flux paths. (a) Front view. (b) Top view. (c) Magnetic flux paths.

As is illustrated in Figure 3c, the magnetic flux lines generated by each turn can be decomposed into six components. Self-inductance is related to the sum of all six components. Mutual inductance is related to the sum of d, e and f. Component f is the source of LMF. Copper loss is mainly affected by components a, b and c.

The geometric parameters influence all six flux components, thereby affecting the system parameters (e.g., k_1 , R_1 and M) to different degrees. Take coil ESR as an example. With the strand diameter of Litz wire being smaller than the skin depth, skin effect is significantly diminished. By contrast, the proximity-effect-induced loss in each strand is caused by the magnetic field strength contributed by all other strands [9,10], including those in the same turn and those that belong to other turns. Therefore, increasing the coil pitch is beneficial for reducing coil ESRs. Meanwhile, when the observation point is located far away from the copper winding, a slight change in coil pitch has a small impact on the winding-to-observation-point distance; hence, mutual inductance and LMF strength are less sensitive to the variation of coil pitch. The same conclusion can be derived from the perspective of the magnetic flux components, i.e., coil pitch has a more significant impact on components a, b and c than on d, e and f.

The complexity in coil assembly optimization lies in the fact that the impacts of the geometric parameters on the FOMs are intertwined; hence, optimizing one single system parameter, e.g., M , does not necessarily guarantee the best overall performance. For instance, minimizing the coil pitch improves M but lowers FOM_{effi} due to the drastically increased coil ESRs, as will be proved in subsequent parts.

3.2. Evaluation of FOMs

3.2.1. Calculation of Coil ESR

FEA is conducted using the Maxwell module in the Ansys Electronics Desktop 2020 R2 suite, from which not only the inductances but also the copper loss in Litz wires is obtainable. The main parameter settings are listed in Table 1.

Table 1. Parameter settings in the Maxwell software.

Parameter	Value
Copper conductivity	5.8×10^7 S/m
Aluminum conductivity	2.7×10^7 S/m
Litz wire diameter	2.45 mm
Litz wire strand diameter	0.1 mm
Litz wire strand number	600
μ_r of ferrite	2200
Coil excitation current	20 A (peak)
Excitation frequency	85 kHz

The ferrite (PC40) core loss density is estimated using the following equation:

$$P_{cv} = 18.7176 f^{1.248} \hat{B}^{2.667} \quad (7)$$

The units of P_{cv} , f and \hat{B} are W/m^3 , Hz and T, respectively. The coefficients are extracted from the loss curves (at 60 degrees Celsius) in the datasheet provided by TDK Inc. (Tokyo, Japan). One can infer from Equation (7) that P_{cv} is roughly proportional to $|I_{coil}|^{2.667}$, where $|I_{coil}|$ is the peak value of the coil current. By contrast, copper loss and eddy loss are roughly proportional to $|I_{coil}|^2$. Accordingly, coil ESR is a monotonically increasing function of $|I_{coil}|$.

The influencing factors of coil ESR include copper loss, core loss and eddy loss. FEA results reveal that coil ESR is insensitive to coil misalignment; hence, it is reasonable to evaluate coil ESR at the zero-misalignment position only. Geometric symmetry can be employed to greatly reduce the runtime. For instance, a quarter model instead of the full model can be used when the coil assembly is symmetrical with respect to the x and y axes.

3.2.2. Evaluation of LMF and Efficiency Performance

The inductances and the LMF strength are directly obtained from the Maxwell software. FEA results show that the LMF strength increases with coil misalignment; hence, the LMF performance in the maximum-misalignment case is of the highest practical value. However, as is explained in Section 2.2, the LMF strength in the zero-misalignment case is also a good indicator of the LMF performance. Therefore, unless otherwise specified, both the efficiency performance and the LMF performance are evaluated at the zero-misalignment case so that symmetry can be employed to greatly reduce the model complexity.

To further save the runtime, a coarser mesh is acceptable during LMF strength calculation and inductance calculation. By contrast, a finer mesh is required to improve the precision of ESR calculation.

3.2.3. Impact of Geometric Parameters

The geometric parameters shown in Figure 4 are varied to reveal their impact on the FOMs. The majority of data are obtained in the zero-misalignment case, except when the impact of coil misalignment is emphasized. The mesh is refined until the results are stable.

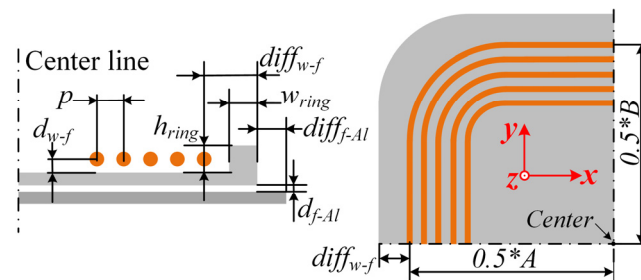


Figure 4. Geometric parameters of the coil assembly (quarter model).

For the sake of simplicity, the rounded corners in the copper winding are omitted in the FEA model. The parameters of the initial design are listed in Table 2. The impacts of geometric parameters on the FOMs are intercoupled, and the impacts are dependent upon the initial point. Therefore, unless otherwise specified, only one parameter deviates from the initial value during the FEA simulations. The TX- and RX-side coil assemblies have identical geometric parameters, except that the aluminum plate size is different.

Table 2. Initial parameters of the coil assembly pair. The unit of all parameters is mm.

Parameter	Value
p	3
A	270
B	270
d_{w-f}	3
d_{f-Al}	2
$diff_{w-f}$	10
$diff_{f-Al}$	5
h_{ring}	0
W_{ring}	5
TX aluminum plate size	$300 \times 300 \times 5$
RX aluminum plate size	$600 \times 600 \times 2$
Ferrite core thickness	5
Air gap height	130

Some of the FEA results are presented in Figure 5. Considering that core loss increases faster than copper loss when the excitation current is increased, core loss is increased tenfold in deriving FOM_{effi2} to simulate significantly higher-power operating conditions. When calculating the FOMs, the units of M , $R_{1/2}$ and $k_{1/2}$ are μH , Ω and $\mu\text{T}/\text{A}$, respectively. The purposes of obtaining these curves are: (1) to reflect how the geometric parameters affect the FOMs and (2) to reveal the different sensitivities of the FOMs to different parameters. The following rules are extracted from FEA results, some of which are not included in Figure 5. It is virtually impossible to quantify the impacts of geometric parameters on the FOMs as the impacts are actually dependent upon the initial point. Therefore, the following conclusions are qualitative.

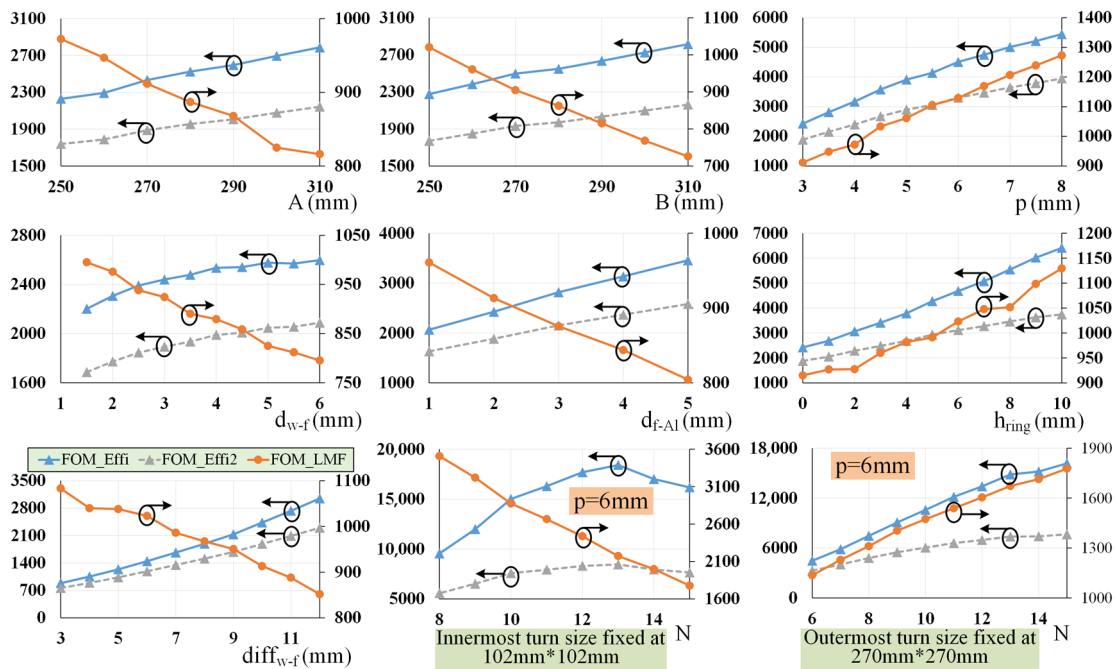


Figure 5. Simulated FOMs. The solid line with triangular dots, dashed line with triangular dots and solid line with circular dots denote FOM_{effi} , FOM_{effi2} and FOM_{LMF} , respectively. For the sake of clarity, the units of the vertical-axis quantities are omitted.

1. With the increase in interlayer distances, (d_{w-f} and d_{f-Al}), FOM_{LMF} is reduced, whereas FOM_{effi} is enhanced.
2. Increasing the coil size (A or B) or the ferrite-coil size difference ($diff_{w-f}$) has the same impacts as increasing d_{w-f} .
3. Adding a ferrite ring, i.e., a protrusion along the outer contour of the ferrite layer, improves both FOMs. By contrast, the impact of w_{ring} is insignificant.
4. The stability of M against coil misalignment can be enhanced via increasing the average turn size of the TX coil. By contrast, increasing the average turn size of the RX coil improves M but has a negligible impact on its stability. In a practical IPT system, higher stability of M means a lighter burden on the power converters, which is favorable. Therefore, the RX coil dimensions should be near the maximum allowable values and the TX coil size should be determined based on the maximum allowable variation of mutual inductance.
5. Increasing the coil pitch (p) is beneficial for improving both FOMs, and the impact is significant. However, for the RX coil, a larger p implies that the maximum allowable turn number is reduced, which can possibly lead to a lower FOM_{effi} . For the TX coil, a larger p means either the turn number or the average turn size is smaller. The possible consequence is either lower FOM_{effi} or lower stability of M , both of which are undesirable. Meanwhile, a lower boundary should be assigned to size of the RX coil's innermost turn. When the innermost turn is so small that its contribution to mutual inductance is far outweighed by its contribution to coil ESR, increasing the turn number not only results in a higher consumption of copper but also lowers FOM_{effi} .
6. When the size of the outermost turn is fixed, increasing the turn number before the size of the innermost turn becomes excessively small is beneficial for improving both FOMs. When the size of the innermost turn and the ferrite core parameters are fixed, both FOMs are decreased after N exceeds a threshold, which is mainly attributable to the increase in eddy loss due to the short distance between the copper winding and the ferrite core boundary. By adding a ferrite ring, the eddy loss can be effectively suppressed, and the maximum allowable size of the outermost turn is increased.

3.2.4. Constraints and Design Parameters

The geometric parameters of the coil assembly pair are subject to various constraints in a practical IPT system. A small profile is preferred for the RX-side coil assembly. By contrast, the TX-side coil should have a relatively large average turn size to improve the stability of M against coil misalignment. Based on Figure 5, the following parameters are fixed to reduce the number of parameter sweeps: $h_{ring} = 7$ mm, $d_{w-f} = 3.2$ mm, $d_{f-Al} = 3$ mm. Increasing h_{ring} is beneficial for enhancing both FOMs. However, after it exceeds a threshold, further increasing h_{ring} results in a larger coil-to-coil distance, which actually lowers FOM_{effi} . d_{w-f} has a smaller impact on FOM_{effi} than on FOM_{LMF} after exceeding 3.5 mm; hence, a relatively small value should be assigned to d_{w-f} . The value of 3.2 mm is equal to sum of the Litz wire radius (1.7 mm) and the insulation layer thickness (1.5 mm) adopted in the inductive charger prototype. d_{f-Al} has a smaller impact on FOM_{LMF} than on FOM_{effi} ; hence, a relatively large value should be adopted. The parameters (listed below) whose impacts on the FOMs are less straightforward are selected as design parameters, i.e., they are to be varied during the manual optimization procedure.

- On the TX side: A , B , p , $diff_{w-f}$;
- On the RX side: p , $diff_{w-f}$, N .

The average turn size of the TX coil is determined by N , p and A (B); hence, the turn number of the TX coil is subject to the restriction on the stability of M and not a free variable.

4. Optimization of Coil Assembly Pair

4.1. Validation of the Accuracy of FEA

Comparisons are made between FEA results and experimental results to verify the accuracy of the former, as is presented in Figure 6. In the FEA model, the coil current has a constant peak value of 20 A. In the experimental measurements, the excitation current provided by the LCR meter (HIOKI IM3536, HIOKI, Nagano, Japan) is 50 mA (rms) and the excitation frequency is 85 kHz. Although both sets of data in Figure 6 do not perfectly match, the overall trend in the FEA results is credible.

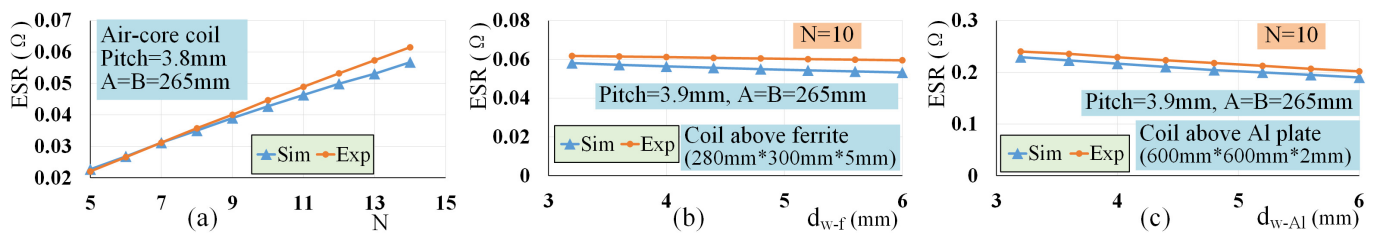


Figure 6. Comparisons between simulated and measured coil ESR. (a) ESR versus N . (b) ESR versus d_{w-f} . (c) ESR versus d_{w-Al} (distance between copper wire and aluminum plate).

4.2. Constraints and Predetermined Parameters

In [17], a manually optimized coil assembly pair with both coil assemblies having identical geometric parameters is compared with the initial design, and the performance improvement is proved via FEA results. This work adopts a more practical design in which the TX-side coil assembly is larger than the RX-side coil assembly. The predetermined parameters and the main constraints are listed in Table 3.

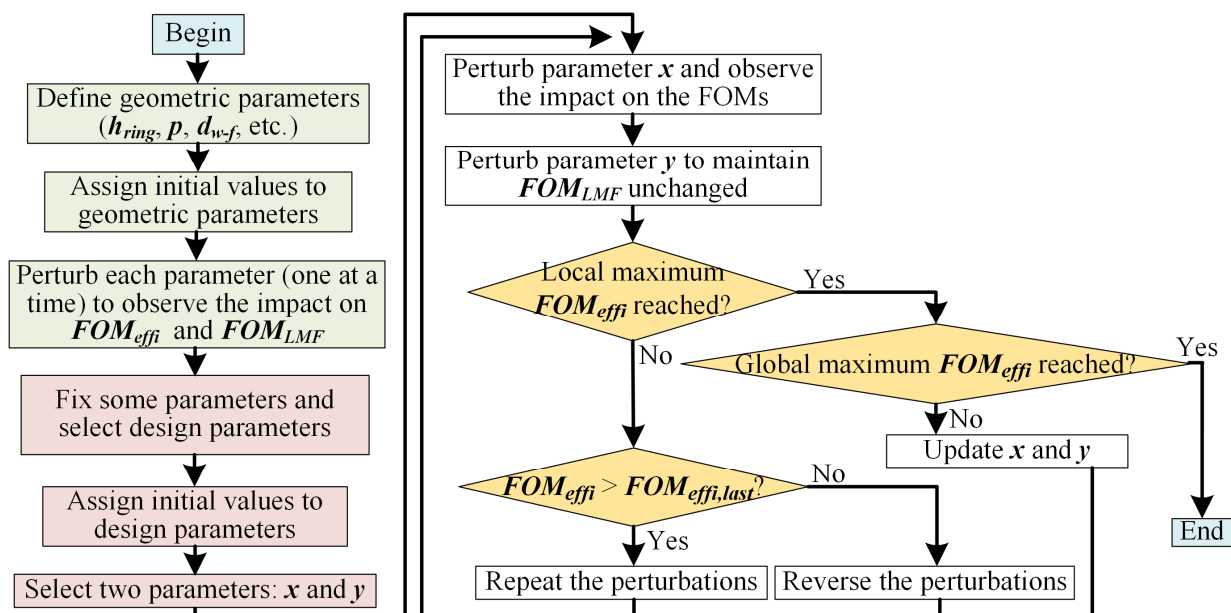
Table 3. Predetermined geometric parameters and constraints of the coil assembly pair. The unit of all parameters is mm.

Parameter	Value
Air gap	160
TX aluminum plate dimensions	$560 \times 560 \times 2$
RX aluminum plate dimensions	$1000 \times 700 \times 2$
TX ferrite core dimensions	$\leq 490 \times 490 \times 5$
RX ferrite core dimensions	$\leq 360 \times 360 \times 5$
Turn number	≤ 18
Coil misalignment	0 to 100

The test bench adopted in this work is capable of moving along one direction (in the horizontal plane) only; hence, coil misalignment is confined to the x axis. The long side of the RX-side aluminum plate is parallel to the x axis.

4.3. Manual Optimization of a Coil Assembly Pair

Based on the conclusions summarized in Section 3.2.3, a manual optimization procedure (illustrated in Figure 7) is conducted. The objective is to maximize FOM_{effi} (subject to the geometric parameter constraints) while having a small impact on FOM_{LMF} . FOM_{LMF} is not prioritized during the optimization procedure because the LMF strength is usually not a major concern in low-power or medium-power IPT systems. As is illustrated in Figure 7, after the impacts of the geometric parameters have been revealed, some parameters are fixed based on a combination of practical constraints and empirical knowledge to reduce the number of parameter sweeps. Meanwhile, the remaining geometric parameters are selected as design parameters during the manual optimization procedure. The selection of design parameters is similar to that introduced in Section 3.2.4. The subscript “last” in Figure 7 denotes the result from the previous test.

**Figure 7.** Flowchart of the manual optimization procedure.

The adjustment of design parameters follows a simple rule: the change in FOM_{LMF} brought by the adjustment of one parameter is offset by the adjustment of another parameter so as to maintain FOM_{LMF} unchanged. If the adjustments result in a higher FOM_{effi} , then continue the perturbation until local maximum is reached for FOM_{effi} . Otherwise, the adjustments to both parameters should be reversed. After the local maximum is achieved,

proceed to perturb another pair of design parameters. The results from the design parameter analysis part serves as a guide, based on which whether the parameter under study should be increased or decreased is determined.

The optimized design and the initial design are shown in Figure 8. The ferrite core is composed of ferrite strips (each measuring 60 mm × 15 mm × 5 mm). Its dimensions are not continuously variable and, thus, slightly deviate from the limit values. The results obtained from FEA (designated as “simulated”), and experimental tests are listed in Table 4. When calculating FOM_{effi} , the units of M and coil ESR are μH and Ω , respectively. The electric parameters are acquired using an LCR meter (HIOKI IM3536, HIOKI, Nagano, Japan) at an excitation current of 50 mA (rms), with the excitation frequency being 85 kHz.

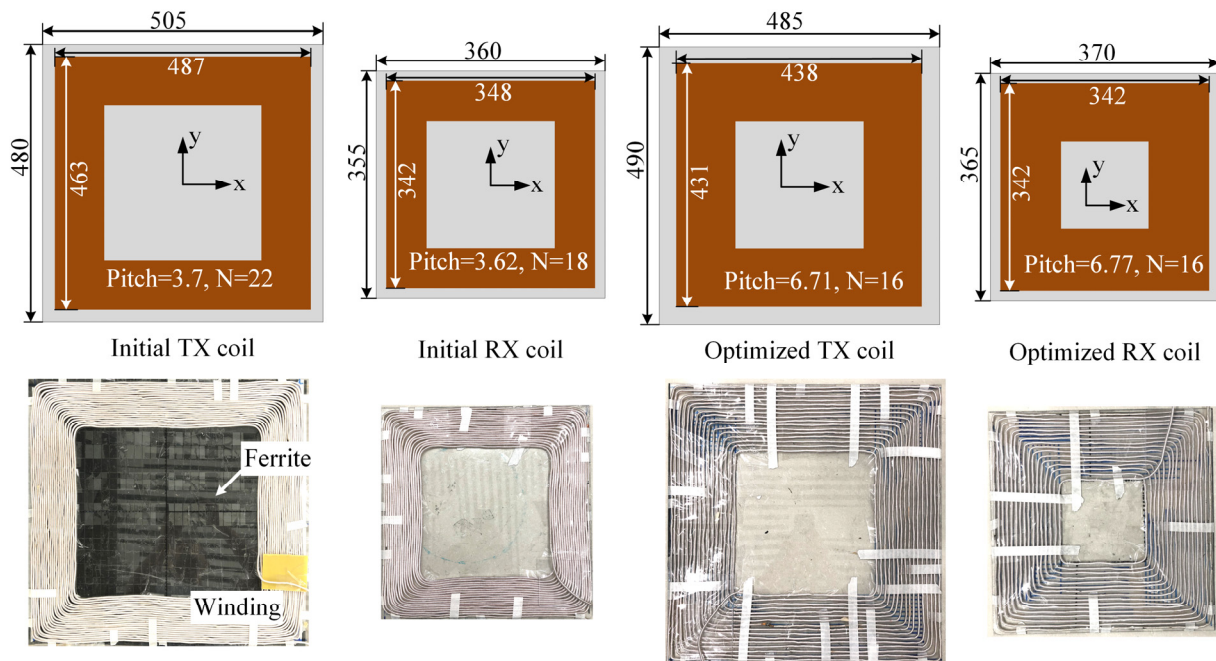


Figure 8. Geometric parameters of the initial and optimized coil assemblies (the aluminum plate is not shown). The coils are made of 600-strand Litz wires.

Table 4. Simulated and measured parameters of the coil assemblies.

Parameter	Initial TX	Initial RX	Optimized TX	Optimized RX
d_{f-Al} (mm)	1.5	1.5	3	3
h_{rng} (mm)	0	0	7	7
Self-inductance (μH)	481.32	223.35	203.25	127.04
DC resistance ($\text{m}\Omega$)	141.0	79.8	88.9	67.5
ESR at 85 kHz ($\text{m}\Omega$)	616.0	295.1	184.2	139.0
Series capacitance (nF)	7.47	15.64	17.76	27.41
Coupling coefficient	0.107 to 0.138		0.137 to 0.187	
Coupling coefficient (simulated)	0.102 to 0.133		0.129 to 0.181	
Mutual inductance (μH)	35.1 to 45.1		22.0 to 30.1	
FOM_{effi}	6780 to 11,193		18,924 to 35,425	
Litz wire length (m)	55.4		36.8	

The disadvantage of the optimized design is that the mutual inductance drop brought by 100 mm coil misalignment (along the x-axis direction) is 27%, whereas in the initial design, the number is 22%. The difference is quite acceptable, though. By contrast, the superiority of the optimized design is obvious. With a 34% reduction in copper wire

consumption, both FOM_{effi} and the coupling coefficient are significantly improved. One can easily infer that the VA rating of the compensation capacitors is greatly reduced.

4.4. Experimental Results

An electric vehicle inductive charger prototype with an operating frequency of 85 kHz is fabricated. The specifications are listed in Table 5. Series compensation is adopted on both sides. The series capacitance values (listed in Table 4) are determined in such a way that the reactance of the coil is almost fully counteracted, and the AC impedance seen by the inverter has a small inductive component. A full-bridge passive rectifier composed of SiC diodes (Rohm SCS220, Rohm, Kyoto, Japan) is adopted on the RX side. A full-bridge inverter composed of SiC MOSFETs (Cree C3M0075120J, Wolfspeed, Durham, NC, USA) is adopted on the TX side. The power and efficiency data are acquired using a power analyzer (HIOKI PW6001, HIOKI, Nagano, Japan). Photographs of the experimental setup are presented in Figure 9.

Table 5. Specifications of the IPT prototype.

Parameter	Value
Litz wire strand diameter (mm)	0.1
Litz wire strand number	600
Ferrite material	PC40
Room temperature (°C)	23–26
DC load resistance (Ω)	15 and 20
Inverter phase shift angle (degree)	180 (fixed)
Input DC-link voltage (V)	100–300 (adjustable)
Inverter switching frequency (kHz)	85 (fixed)
Output power (W)	600
Inverter switching device	Cree C3M0075120J
Rectifier diode	Rohm SCS220

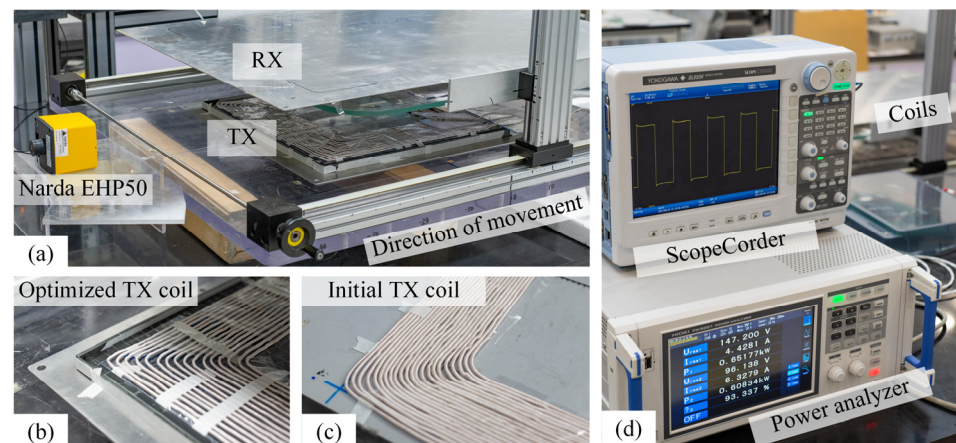


Figure 9. Experimental setup. (a) Coil assembly pair and magnetic field analyzer. (b) Optimized TX coil. (c) Initial TX coil. (d) Measurement of power, efficiency and the inverter's output voltage.

The configuration of the test system is shown in Figure 10. The input DC-link voltage is varied to regulate the output power. The phase shift angle between both half bridges of the inverter is fixed at 180 degrees. Illustrations of the voltage or current waveforms in each stage are also given.

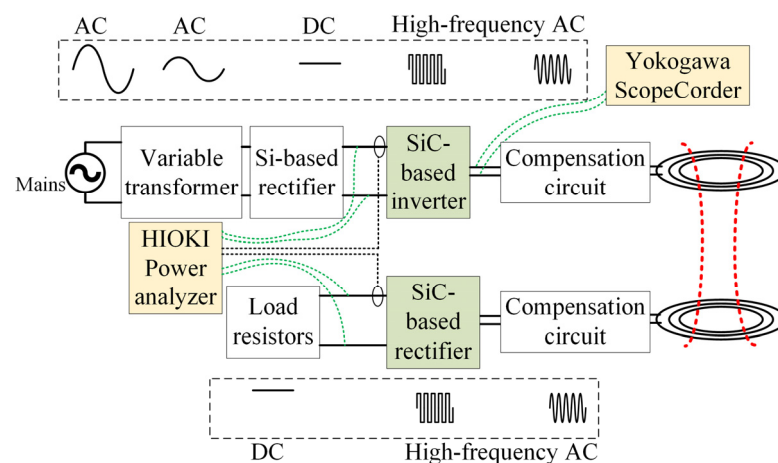


Figure 10. Configuration of the IPT prototype and the voltage or current waveforms. Input power and output power are measured before the SiC-based inverter and after the SiC-based rectifier, respectively.

The LMF strength and the DC-to-DC efficiency are easily measurable, whereas both the FOMs and the coil-to-coil efficiency are more difficult to acquire in the IPT prototype; hence, in this work, the superiority of the optimized design is demonstrated through the measured DC-to-DC efficiency and the LMF strength. The difficulty in measuring the FOMs lies in the fact that the exact coil ESR changes with the excitation current. As the maximum excitation current of the LCR meter (HIOKI IM3536, HIOKI, Nagano, Japan) is merely 50 mA (rms), the ESR data under real operating points, with the current being tens of amperes, are unobtainable. The difficulty in measuring the AC-to-AC efficiency is due to the fact that the measured AC power is sensitive to the phase angle error. For instance, even when the phase compensation value specified in the current sensor's datasheet is used, the measured inverter efficiency may still exceed 100% under some operating points.

Two DC load resistance values are tested: 15 Ω and 20 Ω , which are roughly the optimal load (calculated based on (5)) in the maximum-misalignment and the zero-misalignment cases for the initial design, respectively. The conversion between AC load resistance and DC load resistance is governed by a simple rule: the former is roughly equal to the latter multiplied by $\frac{8}{\pi^2}$. The measured DC-to-DC efficiency at a constant output power of 600 W and the DC-link voltage are given in Figure 11. As is previously stated, the compensation capacitance values are chosen in such a way that the inverter is soft-switched; hence, the inverter loss can be approximated using a small resistance in series with the coil. Figure 11b reveals that the DC-link voltage in the "optimized design" case is lower than that in the "initial design" case, which implies a lower inverter efficiency in the "optimized design" case. One can conclude that even with a lower inverter efficiency, the optimized design results in a higher DC-to-DC efficiency.

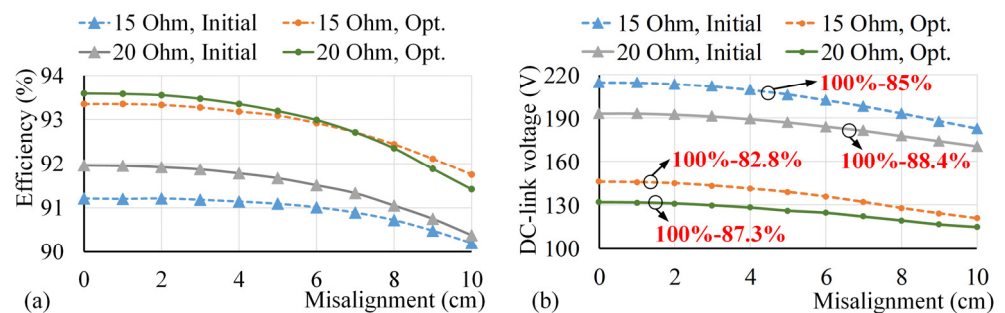


Figure 11. Experimental results. (a) DC-to-DC efficiency. (b) DC-link voltage.

The efficiency improvement brought by the optimization measures is significant. Meanwhile, the stability of mutual inductance, which is reflected in the DC-link voltage curves, is not drastically different in both designs.

The LMF strength is measured using a magnetic field analyzer (Narda EHP50, Narda, Pfullingen, Germany) at a point 70 cm away from the center of the RX coil. The LMF strength measured in the maximum-misalignment case is listed in Table 6. The LMF performance of the optimized design is slightly better.

Table 6. LMF strength measured in the maximum-misalignment case.

DC Load Resistance (Ω)	Initial Design	Optimized Design
15	3.17 μ T	2.94 μ T
20	3.25 μ T	3.11 μ T

5. Discussions

The combination of modern optimization methods and FEA is a useful tool for obtaining the optimal design. However, two shortcomings are obvious. (1) The number of parameter sweeps increases with the number of design parameters. (2) The impact of each design parameter is not explicitly shown, as if the optimization procedure is sealed in a black box. Analytical methods are commonly adopted for their simplicity. However, they are based on simplifications and, thus, unable to deal with complex geometric features. Therefore, these methods are not adopted in this work.

The focus of this work is to construct FOMs for performance assessment of the coil assemblies, analyze the impacts of geometric parameters on the FOMs and propose practical measures to improve FOM_{effi} . After the impacts are clearly revealed, one no longer needs to rely on modern optimization methods to yield the optimal design. In this work, manual optimization (illustrated in Figure 7) is adopted. Comparisons between this work and some relevant works in the literature are given in Table 7.

Table 7. Comparisons between this work and relevant works in the literature.

Reference	Inclusion of Ferrite Core	Inclusion of Aluminum Shield	Number of Parameter Sweeps	Analytical or Numerical	Impact of Design Parameters Explicitly Shown
[14]	No	No	Not applicable	Analytical	No
[9]	Yes	No	Not applicable	Analytical	No
[13]	Yes	No	Small	Analytical	No
[10]	Yes	No	Large	Hybrid	No
[8]	Yes	No	Large	Numerical	No
This work	Yes	Yes	Moderate	Numerical	Yes

In [14], only the copper winding is included in the analytical model, whereas the ferrite core and the aluminum shield plate are not considered. As a result, this model is suitable for a narrow range of applications. In [8–10,13], the ferrite core is considered in the model but the aluminum shield plate is omitted. Analytical, numerical or hybrid (partially analytical and partially numerical) approaches are adopted to construct these models. Depending on the concrete methodology, the number of parameter sweeps varies greatly. Analytical models generally require fewer parameter sweeps. None of these four references attempted to explicitly reveal the impact of the design parameters. This work takes a numerical approach and attempts to explicitly reveal the impact of the design parameters on the performance. Both the ferrite core and the aluminum shield plate are considered. By using the manual optimization method introduced in Figure 7, the number of parameter sweeps is effectively reduced.

Provided that both the FEA software and the model parameters are accurate, one can have confidence in the accuracy of FEA results. Due to unavoidable errors in the geometric and electrical parameters, the FEA results do not strictly match experimentally

measured data in this work. Still, the general trend in the FEA results is credible. The DC load resistance adopted in the prototype ($15\ \Omega$ and $20\ \Omega$) is chosen in such a way that it is equal to the theoretical optimal values for the initial design. For the optimized design, the numbers are approximately $13\ \Omega$ and $17\ \Omega$, respectively. The impact of load resistance is clearly displayed in Figure 11. Therefore, one can conclude that even with a non-optimal load resistance, the optimized design still outperforms the initial design by a noticeable margin in terms of efficiency and by a small margin in terms of LMF performance.

The key measures for coil assembly optimization are summarized as follows. (1) Coil pitch should be increased to a suitable level to reduce coil ESRs. (2) The average turn size of the TX coil is determined by the required stability of mutual inductance. (3) A ferrite ring should be added and the distance between the outermost turn of the copper winding and the boundary of the ferrite core should be reasonably large to reduce eddy loss.

The findings of this work are applicable to IPT systems other than electric vehicle inductive chargers, as no restrictions specific to electric vehicle charging are imposed during the analysis and optimization procedures. Besides, some of the optimization measures can be applied to coil designs other than the single-winding rectangular type.

6. Conclusions

Two FOMs are proposed for evaluating the performance of coil assemblies applied in electric vehicle inductive charging applications. The impacts of the main geometric parameters on both FOMs are examined with the aid of finite element analysis. A manual optimization procedure is conducted based on the qualitative rules extracted from FEA results. In the optimized design, both FOM_{effi} and the coupling coefficient are enhanced. The copper wire consumption is reduced. The LMF strength is slightly lowered. The superior performance of the optimized design is proved via FEA results and experimental tests conducted on an electric vehicle inductive charger prototype. The key measures for coil assembly optimization are summarized.

Author Contributions: Conceptualization, G.Z.; methodology, G.Z.; software, G.Z.; validation, G.Z.; formal analysis, G.Z.; investigation, G.Z.; resources, D.G.; data curation, G.Z.; writing—original draft preparation, G.Z.; writing—review and editing, D.G.; visualization, G.Z.; supervision, D.G.; project administration, D.G.; funding acquisition, D.G. All authors have read and agreed to the published version of the manuscript.

Funding: This research was funded by Beijing Natural Science Foundation, grant number 3212030. The APC was funded by Beijing Natural Science Foundation, grant number 3212030.

Conflicts of Interest: The authors declare no conflict of interest.

References

- Dai, X.; Li, X.; Li, Y.; Hu, A.P. Maximum Efficiency Tracking for Wireless Power Transfer Systems with Dynamic Coupling Coefficient Estimation. *IEEE Trans. Power Electron.* **2018**, *33*, 5005–5015. [\[CrossRef\]](#)
- Zhu, G.; Gao, D.; Lin, S. Leakage Magnetic Field Suppression Using Dual-Transmitter Topology in EV Wireless Charging. *J. Power Electron.* **2019**, *19*, 625–636.
- Mohammad, M.; Choi, S.; Elbuluk, M. Loss Minimization Design of Ferrite Core in a DD-Coil-based High-Power Wireless Charging System for Electrical Vehicle Application. *IEEE Trans. Transp. Electrif.* **2019**, *4*, 957–967. [\[CrossRef\]](#)
- Budhia, M.; Covic, G.A.; Boys, J.T.; Huang, C.-Y. Development and Evaluation of Single Sided Flux Couplers for Contact-less Electric Vehicle Charging. In Proceedings of the 2011 IEEE Energy Conversion Congress and Exposition, Phoenix, AZ, USA, 17–22 September 2011.
- Tang, Y.; Zhu, F.; Ma, H. Efficiency Optimization with a Novel Magnetic-Circuit Model for Inductive Power Transfer in EVs. *J. Power Electron.* **2018**, *1*, 309–322.
- Otomo, Y.; Igarashi, H. A 3-D Topology Optimization of Magnetic Cores for Wireless Power Transfer Device. *IEEE Trans. Magn.* **2019**, *55*, 1–5. [\[CrossRef\]](#)
- Al-Saadi, M.; Valtchev, S.; Gonçalves, J.; Crăciunescu, A. New Analytical Formulas for Coupling Coefficient of Two Inductively Coupled Ring Coils in Inductive Wireless Power Transfer System. In Proceedings of the 7th EAI International Conference, GreeNets 2020, Harbin, China, 27–28 June 2020; pp. 117–127.
- Yilmaz, T.; Hasan, N.; Zane, R.; Pantic, Z. Multi-Objective Optimization of Circular Magnetic Couplers for Wireless Power Transfer Applications. *IEEE Trans. Magn.* **2017**, *53*, 1–12. [\[CrossRef\]](#)

9. Hariri, A.; Elsayed, A.; Mohammed, O.A. An Integrated Characterization Model and Multiobjective Optimization for the Design of an EV Charger's Circular Wireless Power Transfer Pads. *IEEE Trans. Magn.* **2017**, *53*, 1–4. [[CrossRef](#)]
10. Bosshard, R.; Kolar, J.W. Multi-Objective Optimization of 50 kW/85 kHz IPT System for Public Transport. *IEEE J. Emerg. Sel. Topics Power Electron.* **2016**, *4*, 1370–1382. [[CrossRef](#)]
11. Kim, M.; Park, S.; Jung, H.-K. Numerical Method for Exposure Assessment of Wireless Power Transmission under Low-Frequency Band. *J. Magn.* **2016**, *21*, 442–449. [[CrossRef](#)]
12. Park, S. Evaluation of Electromagnetic Exposure During 85 kHz Wireless Power Transfer for Electric Vehicles. *IEEE Trans. Magn.* **2018**, *54*, 1–8. [[CrossRef](#)]
13. Lu, M.; Ngo, K.D.T. A Fast Method to Optimize Efficiency and Stray Magnetic Field for Inductive-Power-Transfer Coils Using Lumped-Loops Model. *IEEE Trans. Power Electron.* **2018**, *33*, 3065–3075. [[CrossRef](#)]
14. Sampath, J.P.K.; Alphones, A.; Vilathgamuwa, D.M. Coil optimization against misalignment for wireless power transfer. In Proceedings of the 2016 IEEE 2nd Annual Southern Power Electronics Conference (SPEC), Auckland, New Zealand, 5–8 December 2016; pp. 1–5.
15. Wang, X.; Sun, P.; Deng, Q.; Wang, W. Evaluation of AC Resistance in Litz Wire Planar Spiral Coils for Wireless Power Transfer. *J. Power Electron.* **2018**, *18*, 1268–1277.
16. Yashima, Y.; Omori, H.; Morizane, T.; Kimura, N.; Nakaoka, M. Leakage magnetic field reduction from Wireless Power Transfer system embedding new eddy current-based shielding method. In Proceedings of the 2015 International Conference on Electrical Drives and Power Electronics (EDPE), Tatranska Lomnica, Slovakia, 21–23 September 2015; pp. 241–245.
17. Zhu, G.; Gao, D. Finite Element Analysis-Aided Performance Improvement of Circular Coil Assemblies Applied in Electric Vehicle Inductive Chargers. In Proceedings of the 2021 International Conference on Wireless Power Transfer, 34th International Electric Vehicle Symposium and Exhibition (EVS34), Nanjing, China, 25–28 June 2021.